Article:
Ketchen, S, Rohwedder, A, Knipp, S et al. (2020) A novel workflow for three-dimensional analysis of tumour cell migration. Interface Focus, 10 (2). 20190070. ISSN: 2042-8898

https://doi.org/10.1098/rsfs.2019.0070

INTERFACE FOCUS

A novel workflow for 3D analysis of tumour cell migration

Journal:	*Interface Focus*
Manuscript ID	RSFS-2019-0070.R2
Article Type:	Research
Date Submitted by the Author:	09-Nov-2019
Complete List of Authors:	Ketchen, Sophie; University of Leeds Faculty of Medicine and Health Rohwedder, Arndt; University of Leeds Faculty of Biological Sciences Knipp, Sabine; University of Leeds Faculty of Biological Sciences Esteves, Filomena; University of Leeds Faculty of Medicine and Health Struve, Nina; University Medical Center Hamburg-Eppendorf, Laboratory of Radiobiology & Experimental Radiation Oncology Peckham, Michelle; University of Leeds Faculty of Biological Sciences Ladbury, John; University of Leeds Faculty of Biological Sciences Curd, Alistair; University of Leeds Faculty of Biological Sciences Short, Susan; University of Leeds Faculty of Medicine and Health Bruning-Richardson, Anke; University of Huddersfield School of Applied Sciences,
Subject:	Biocomplexity < CROSS-DISCIPLINARY SCIENCES, Biochemistry < CROSS-DISCIPLINARY SCIENCES, Bioinformatics < CROSS-DISCIPLINARY SCIENCES
Keywords:	3D, tumour spheroid, microscopy, ImageJ, cell migration

Author-supplied statements

Relevant information will appear here if provided.

Ethics

Does your article include research that required ethical approval or permits?:
This article does not present research with ethical considerations

Statement (if applicable):
CUST_IF_YES_ETHICS :No data available.

Data

It is a condition of publication that data, code and materials supporting your paper are made publicly available. Does your paper present new data?:
Yes

Statement (if applicable):
There is a link to the developed Plugin in the text. We are happy to share data.

Conflict of interest

I/We declare we have no competing interests

Statement (if applicable):
CUST_STATE_CONFLICT :No data available.

Authors' contributions

This paper has multiple authors and our individual contributions were as below

Statement (if applicable):
SK carried out the lab work, participated in data analysis, participated in the design of the study and drafted the manuscript; AR designed the ImageJ plugin, participated in the design of the study, acquisition of the data, analysis of the data and critically revised the manuscript; SKnipp contributed to data acquisition and critically revised the manuscript; FE participated in the design of the cell staining method and critically revised the manuscript; NS participated in the design of the cell staining method and critically revised the manuscript; MP participated in the design of the study and critically revised the manuscript; JEL participated in the interpretation of the data and critically revised the manuscript; AC participated in the design of the study, acquisition of the data, analysis of the data, interpretation of the data and critically revised the manuscript; SCS participated in the design of the study and critically revised the manuscript; ABR conceived of the study, designed the study, coordinated the study and helped draft the manuscript. All authors gave final approval for publication and agree to be held accountable for the work performed therein.

A novel workflow for 3D analysis of tumour cell migration

Sophie Ketchen[1], Arndt Rohwedder[2], Sabine Knipp[2], Filomena Esteves[1], Nina Struve[3], Michelle Peckham[2], John E. Ladbury[2], Alistair Curd[2], Susan C. Short[1], Anke Brüning-Richardson[4]

[1] Leeds Institute of Cancer and Pathology, University of Leeds, Leeds, UK

[2] School of Molecular and Cellular Biology, University of Leeds, Leeds, UK

[3] Laboratory of Radiobiology & Experimental Radiation Oncology, Hubertus Wald Tumorzentrum – University Cancer Center Hamburg, University Medical Center Hamburg-Eppendorf, Hamburg, Germany

[4] School of Applied Sciences, University of Huddersfield, Huddersfield, UK

Keywords

3D, tumour spheroid, microscopy, ImageJ, cell migration

Abstract

The limitations of two-dimensional (2D) analysis in three-dimensional (3D) cellular imaging impair the accuracy of research findings in biological studies. Here we report a novel 3D approach to acquisition, analysis and interpretation of tumour spheroid images. Our research interest in mesenchymal-amoeboid transition led to the development of a workflow incorporating the generation and analysis of 3D data with Instant Structured Illumination Microscopy and a new ImageJ plugin.

Main Text

Traditionally cancer drug screens have relied on the assessment of drug activity on 2D cell monolayers quantifying cytotoxic effects. The advantages of this approach are clear and include high throughput screening, determination of direct effects on cell viability and advancing our understanding of cancer biology [1]. However, the disappointing hit rate of drug discovery when translated into clinical trials has highlighted the importance of targeting cancer cells in a setting more appropriate for recapitulating the 3D structure of an original tumour [2]. In addition, there has been a steady increase in the development of anti-migratory drugs as adjuvant treatment to target the dissemination of highly invasive cancers such as gliomas. Screening of cells migrating in a 3D environment is more likely to provide a more accurate assessment of drug activity than within a 2D environment [3].

In our own drug screens of novel anti-migratory drugs in 3D spheroid migration assays, we recently identified a small molecule inhibitor, CCG-1423, that appears to promote distinct cellular responses in highly migratory glioma cells. CCG-1423 targets the RhoA transcription signalling pathway [4] and seemingly induces a mesenchymal-

amoeboid transition (MAT) in treated cells. Mesenchymal and amoeboid modes of migration are interchangeable as switching between the two can be induced in cancer cells in response to changes in the extracellular environment including external pressures such as drug selection [5]. This cellular switch may potentially allow the identification of pathways involved in this mechanism and enhance drug development. This is extremely important as a combination approach targeting both migration modes may be required to fully stop migratory activity in cancer cells.

In terms of tumour architecture and cell migration, using 3D cell cultures embedded in collagen is a more appropriate method to screen the action of drugs. In our own work (unpublished data), we found cells in 2D monolayers appeared to have a much higher sensitivity to the drug CCG-1423 compared to 3D cell cultures using live cell imaging. However, this type of assessment relies on the interpretation of 2D images created by light microscopy from, for example, 3D spheroid invasion assays. The interpretation of such images has to be treated with caution, as there are several limitations to their assessment. For example, important details of drug activity could be missed because images are only captured in a single focal plane at any given time, potentially leading to an overestimation of drug efficacy. Thus, there is a strong need for better high-resolution analysis of 3D image data, which is less well developed than analysis in 2D.

To investigate the effect of CCG-1423 treatment on glioma cells at higher resolution and in 3D, we used Instant Structured Illuminated Microscopy (iSIM), which captures images at high spatio-temporal resolution (~150 nm, > 100 fps), allowing rapid capture of high-resolution volumes (Z-stacks) [6][7]. Having labelled spheroids encased in collagen (see Methods/Supplementary), we acquired 3D images of single migratory

cells. While brightfield images indicated that the inhibitor caused the cells to adopt a rounded phenotype, a key feature of amoeboid migration (Figure 1A), iSIM (Figure 1B) allowed us to observe morphological features in fine detail, including actin bundles. This detail alone allowed us to enhance our understanding of CCG-1423 drug activity on cell migration as we could more closely observe its direct effects on actin dynamics and cytoskeletal rearrangements.

To aid in the analysis of the 3D spheroids, we developed, and provide here a novel ImageJ plugin to quantify morphological features relevant to cellular migration (Figure 2). The plugin was used to calculate the number of major protrusions, such as lamellipodia, and small protrusions such as filopodia in the cells under treated versus untreated conditions. Lamellipodia are large, actin-based, sheet-like cellular protrusions involved in cell movement, whilst filopodia are thin, actin-rich cellular protrusions that emerge from the lamellipodia allowing a cell to probe and interact with its environment, promoting cell migration. The formation of both types of feature is regulated by the activity of small Rho GTPases, Rac1 and CDC42, orchestrators of MAT [8]. There was a distinct loss of major protrusions/lamellipodia in treated cells concurrent with an increase in the number of filopodia, a striking feature of MAT (Figure 3). Our results support a direct effect on actin dynamics and cell morphology indicative of MAT when cells are treated with CCG-1423.

This analysis could potentially be adapted for use in routine screening with fully automated high-content imaging systems such as the Operetta (Perkin Elmer). It will be interesting to ascertain whether such images have sufficient resolution for our post-

processing technique. On the other hand, iSIM may be developed for automated screening over a 96-well format.

While the current plugin works well, there are a couple of limitations that the user should be aware of. First, cell-cell proximity can be a limiting factor in the analysis method. Only the largest object will be analysed per slice in a 3D FOV. Where multiple cells are present, without the cells being connected to each other, the per-slice analysis method may therefore swap between cells as it moves through a Z-stack. Further development may improve on this limitation, allowing for faster data acquisition from multiple cells simultaneously, and maintaining the association between analysis results and particular cells. On the other hand, when multiple cells are connected in a cluster, protrusions from the whole cluster will be identified, which will provide useful data. Second, protrusions are detected in each slice of a 3D image, analysed separately, and there is no output information about the direction of protrusions in the Z-direction. Further development will improve on this analysis to provide more information relevant to 3D cell migration.

In conclusion, our combined workflow of sample preparation, iSIM image acquisition and application of a novel ImageJ analysis plugin allowed us to confirm a proposed phenotype switch in migrating glioma cells after treatment with the inhibitor CCG-1423 in 3D environments. We detected a significant decrease in the number of major protrusions in treated cells. This supports the idea that amoeboid cells display a more rounded morphology, as they undergo MAT. In addition, amoeboid cells typically present smaller protrusions, which may explain the observed increase in the number of filopodia in CCG-1423 treated cells. We propose that this type of analysis can be

used for many cell types, including primary tumour explants, and may be applicable to other investigations of detailed phenotypic changes and protein localisation in a 3D setting. In our own studies using a whole range of inhibitors targeting the actin polymerisation pathway, we observed very specific phenotypes in response to the different inhibitors (unpublished data). This shows the potential of this method in assessing a range of cellular responses to different pharmacological agents. In addition to MAT investigations, this analysis could also be used for the reciprocal process of amoeboid to mesenchymal transition (AMT). The analysis would be exactly the same as for MAT, however the predicted results would be reversed with an increase in major protrusions and a decrease in filopodia. Morphologically, the cells would change from rounded to elongated as they transitioned from an amoeboid to a mesenchymal phenotype.

Gliomas are often treated with radiation in addition to chemotherapy drugs. The determination of the optimum clinical target volume margins around gross tumour volume is possibly the most uncertain stage in the planning of a radiotherapy regimen in any cancer treatment but in brain cancer, it requires even more extensive research [9]. The study of 3D models/spheroids could potentially open new avenues in the management of gliomas with chemo-radiotherapy through a better understanding of cellular behaviour and intervention using anti-migratory drugs. Thus, reducing cell migration could produce more defined tumour margins resulting in accurate radiotherapy and enhanced glioma treatment. In the context of our own research, we have generated confirmatory and additional information to support the need for combination treatments to target both mesenchymal and amoeboid cell migration to fully prevent glioma cell migration and invasion.

Methods

***In vitro cultures*.** The established glioma cell line U251 was cultured at 37°C in a 5% CO_2 incubator (Sanyo) in high glucose DMEM (Sigma, UK) supplemented with 10% heat-inactivated FCS (Labtech, UK) and Pen/Strep (Sigma, UK) in plastic tissue culture flasks (Corning).

***3D spheroid generation and invasion assay*.** For inhibitor studies, U251 cells were seeded at $1x10^3$/well in low adherence 96 well plates (Nunc, UK) as previously described [10]. Three days after seeding, spheroids contained within the wells were embedded in rat tail collagen V (Corning Life Science, US), polymerisation was achieved with 1M NaOH. The inhibitor CCG-1423 (Tocris Bioscience, US) was resuspended in DMSO and was added at a predetermined anti-migratory concentration (500nM). Some spheroids were mock-treated with DMSO-supplemented medium only. Invasion into collagen was observed over 72 hours at 24-hour interval and images captured with the EVOS Cell Imaging System (Advanced Microscopy Group) at 4x magnification.

***Preparation of spheroids and migratory cells for iSIM imaging*.** We have previously reported the staining of collagen embedded spheroids and associated migratory cells with fluorescent dyes such as phalloidin and DAPI [10]. Here we optimised this technique to allow antibody labelling. The whole procedure was adapted so that it can be carried out in the original low adherence 96-well plate (Nunc, US). After completion of the invasion assay, the wells were carefully washed with PBS three times; this was achieved using 200µl pipette tips and pastettes to add and remove

fresh PBS. The collagen plugs were then fixed using 4% PFA for 40 minutes. For permealisation, 0.5% Triton-X100 was added for 30 minutes; three washes of PBS were followed by blocking with 0.01% Marvel skimmed milk powder in PBS for five minutes. The collagen plugs were then incubated with Alexa Fluor 488 phalloidin at 1/500 (Molecular probes, Invitrogen US) and anti-acetylated tubulin antibody (1/500) (Abcam, UK), which had been prepared in the blocking solution (0.01% Marvel skimmed milk powder) and spun down for 5 minutes at 13,000 rpm. After a two-hour incubation, the collagen plugs were washed three times with PBS for five minutes each; the secondary antibody, anti-mouse Alexa Fluor 594 preadsorbed (1/500; Molecular probes, Invitrogen US), was added at a 1/500 concentration along with DAPI (1/500, according to manufacturer instructions), prepared as for the primary antibody solution. Incubation was for 1 hour after which the collagen plugs were washed three times with PBS. The collagen plugs were carefully lifted out of the wells and transferred onto glass slides. Fluoromount G (Thermo Fisher Scientific, UK) was added to the plugs and coverslips were gently lowered onto the collagen plugs.

iSIM imaging. The iSIM used for this study was home-built at the University of Leeds [6]. The objective lens used was a x60 NA 1.2 objective (Olympus). Z-stacks were acquired at 50 ms per slice. Deconvolution was performed on all final images using the Image plugin DeconvolutionLab (Biomedical Imaging Group, EPFL, Switzerland). Depth-colour coding used a modified version of K_TimeRGBcolorcode.ijm (ImageJ macro by Kota Miura, Centre for Molecular and Cellular Imaging, EMBL Heidelberg, Germany).

ImageJ plugin for data analysis. The plugin developed and used in this study is 'Surface and DirectionDetector B' v1.0, available at https://github.com/rohwedderleeds/surfaceanalyser.

Briefly, in each FOV, or each Z-slice of a 3D image, the cell outline (perimeter) is identified and a smoothened perimeter is generated. The centre of mass for this smoothened perimeter is used as the position of the cell centre. Values for the distance to the cell centre (radii) are stored as a function of position on the cell outline. According to sensitivity limits (larger windows for larger protrusions, smaller windows for smaller protrusions or filopodia), a sliding slope estimate for change in radius against position on the outline is applied and stored as a series of b-values. Slopes are then calculated in the same way in the reversed direction around the cell outline. The ratio and product of these two *b*-series allow the detection and localisation of protrusions, respectively (see supplementary material). Eccentricity is calculated as the distance between the centre of mass for the cell outline and the centre of mass for the smoothened perimeter. The procedure can be applied to 2D images (Figure 2A) and 3D image stacks (Figure 2B) and generates outputs for both cases. The output consists of the graphical representation of the major protrusions, a log containing the measured eccentricity and protrusion counts, and the tables of major protrusions and filopodia, in separate windows. Further details of the analysis method can be found in the supplementary section.

Supplementary Material

See Supplementary Figs. 1 and 2. The ImageJ plugin takes the current image/image stack and generates an internal copy for the analysis. In the case of an image stack, each slice is evaluated individually. Upon call, a graphical user interface (GUI) opens

to enter values for the estimated image coverage of the cell under consideration, and the size of the major and minor (referred to as filopodia) protrusions as a percentage of the total cell outline. The remaining procedure runs in the background and does not require any user activity.

Firstly, an object (e.g. cell) outline is obtained as follows. A black and white image is first generated using auto-threshold. To remove single pixel noise and the effect of small fluorescent particles on the analysis, a rank filter is applied to the image using median and bright outliers filters. The function ParticleAnalyser is then used for isolating the cell/cluster of cells. It uses the options EXCLUDE_EDGE_PARTICLES, requiring objects not touching the frame, INCLUDE_HOLES, resulting in the detection of the outer objects border only and CENTER_OF_MASS, which is used for calculating eccentricity of the object. The particle analyser will try to find an object with a size greater than the minimum size estimated by the user in the GUI. If it fails, it reduces the minimum size value until an object is identified. When multiple cells are present in a FOV, if they are separate from one another, the largest cell will be automatically identified; if the cells are connected in a cluster, the whole cluster will be selected as the object and analysed for its major and minor protrusions. When an object is found, its outline is stored for analysis as a linear array of pixel coordinates. A rounded perimeter is generated from a sliding average of the object outline (red ellipse in Supplementary Fig. 1). In a single cell, this is used to approximate the cell body, containing the nucleus. Eccentricity (E in Supplementary Fig. 1) is calculated as the distance between the centre of mass of the cell outline (blue circle in Supplementary Fig. 1) and the centre of mass of the rounded perimeter (the ‘cell centre’).

For each pixel on the cell outline, its position in pixels along the outline (x) and a radius (r) is stored. $r(x)$ is the Euclidean distance from the cell centre to the cell outline at position x along the cell outline. Based on the protrusion size entered into the GUI, for both major and minor protrusions, a sliding linear regression ($r = a + bx$) is applied, giving

$$b_i = \frac{n_{window}\left(\sum_{j=i}^{i+window} x_j r_j\right) - \sum_{j=i}^{i+window} x_j \sum_{j=i}^{i+window} r_j}{n_{window}\left(\sum_{j=i}^{i+window} x_j r_j\right) - \left(\sum_{j=i}^{i+window} x_j r_j\right)^2},$$

where b_i is the average slope over n_{window} pixels along the outline, at the ith pixel position along the cell outline.

The algorithm is applied bi-directionally by inverting the r array order, so that

$$r_{inv} = (y_N, y_{N-1}, \ldots y_1),$$

where N is the length of the cell outline in pixels. b_{inv} then results from the sliding regression applied to r_{inv}, and a second inversion, this time of b_{inv}, maps the slopes obtained in the reversed direction around the outline back to the original positions (x) along the outline:

$$b_{inv_{inv}} = (b_{inv_N}, b_{inv_{N-1}} \ldots b_{inv_1}).$$

The ratio between b and $b_{inv_{inv}}$ is calculated for each position along the cell outline:

$$b_{ratio}(x) = \frac{b(x)}{b_{inv_{inv}}(x)}.$$

This b-ratio (green in Supplementary Fig. 1) generates a strong accentuation of protrusions, as shown in Supplementary Fig. 1. The bi-directionality in the calculation also allows a narrower estimate of the actual position than a sliding regression in only one direction around the cell.

Upon reaching the sensitivity threshold for the *b*-ratio (Supplementary Fig. 1: GUI input and dashed black line), a protrusion is detected. The location of the maximum of the *b*-product, the element-wise product of b and $b_{inv_{inv}}$ (absolute value, blue in Supplementary Fig. 1), in between one such detection and the following detection, provide the location (*x*) along the outline of the protrusion. Output is provided as noted in Methods.

Author Contributions

SK carried out the lab work, participated in data analysis, participated in the design of the study and drafted the manuscript; AR designed the ImageJ plugin, participated in the design of the study, acquisition of the data, analysis of the data and critically revised the manuscript; SKnipp contributed to data acquisition and critically revised the manuscript; FE participated in the design of the cell staining method and critically revised the manuscript; NS participated in the design of the cell staining method and critically revised the manuscript; MP participated in the design of the study and critically revised the manuscript; JEL participated in the interpretation of the data and critically revised the manuscript; AC participated in the design of the study, acquisition of the data, analysis of the data, interpretation of the data and critically revised the manuscript; SCS participated in the design of the study and critically revised the manuscript; ABR conceived of the study, designed the study, coordinated the study and helped draft the manuscript. All authors gave final approval for publication and agree to be held accountable for the work performed therein.

Acknowledgements:

We would like to thank the PPR Foundation and MRC for funding.

Data Accessibility:

The plugin developed and used in this study is 'Surface and DirectionDetector B' v1.0, available at https://github.com/rohwedderleeds/surfaceanalyser.

Funding

This work was supported by The PPR Foundation [RGCALA106893-002] and the MRC [MR/K015613/1].

References

1. Haglund C, Aleskog A, Nygren P, Gullbo J, Höglund M, Wickström M, Larsson R, Lindhagen E. 2012 In vitro evaluation of clinical activity and toxicity of anticancer drugs using tumor cells from patients and cells representing normal tissues. *Cancer Chemother. Pharmacol.* **69**, 697–707. (doi:10.1007/s00280-011-1746-1)

2. Jardim DL, Groves ES, Breitfeld PP, Kurzrock R. 2017 Factors associated with failure of oncology drugs in late-stage clinical development: A systematic review. *Cancer Treat. Rev.* **52**, 12–21. (doi:10.1016/j.ctrv.2016.10.009)

3. Baumann K. 2010 Moving in 3D. *Nat. Rev. Mol. Cell Biol.* **11**, 465.

4. Evelyn CR, Wade SM, Wang Q, Wu M, Iñiguez-Lluhí JA, Merajver SD, Neubig RR. 2007 CCG-1423: a small-molecule inhibitor of RhoA transcriptional signaling. *Mol. Cancer Ther.* **6**, 2249–2260. (doi:10.1158/1535-7163.MCT-06-0782)

5. Paňková K, Rösel D, Novotný M, Brábek J. 2010 The molecular mechanisms of transition between mesenchymal and amoeboid invasiveness in tumor cells. *Cell. Mol. Life Sci.* **67**, 63–71. (doi:10.1007/s00018-009-0132-1)

6. Curd A, Cleasby A, Makowska K, York A, Shroff H, Peckham M. 2015 Construction of an instant structured illumination microscope. *Methods San Diego Calif* **88**, 37–47. (doi:10.1016/j.ymeth.2015.07.012)

7. York AG, Chandris P, Nogare DD, Head J, Wawrzusin P, Fischer RS, Chitnis A, Shroff H. 2013 Instant super-resolution imaging in live cells and embryos via analog image processing. *Nat. Methods* **10**, 1122–1126. (doi:10.1038/nmeth.2687)

8. Mattila PK, Lappalainen P. 2008 Filopodia: molecular architecture and cellular functions. *Nat. Rev. Mol. Cell Biol.* **9**, 446–454. (doi:10.1038/nrm2406)

9. Moghaddasi L, Bezak E, Marcu LG. 2012 Current challenges in clinical target volume definition: tumour margins and microscopic extensions. *Acta Oncol. Stockh. Swed.* **51**, 984–995. (doi:10.3109/0284186X.2012.720381)

10. Cheng V, Esteves F, Chakrabarty A, Cockle J, Short S, Brüning-Richardson A. 2015 High-content analysis of tumour cell invasion in three-dimensional spheroid assays. *Oncoscience* **2**, 596–606.

Figure Legends

Figure 1. Imaging of U251 glioma cells and spheroids.

A. Brightfield images of U251 glioma cells after 72h hours incubation, embedded in collagen, in 96-well low adherent plates. Untreated spheroid and spheroid treated with the small molecule inhibitor CCG-1423. The arrows indicate migratory cells in both untreated and CCG-1423 treated cells. In the untreated spheroids elongated cells are visible migrating into the collagen, whereas in the treated spheroids the morphology has seemingly changed to a more rounded phenotype. Scale bar = 1000μm (original image, top), 250μm (magnified region, bottom).

B. High resolution 3D iSIM imaging of fixed spheroids and migrating cells within the collagen plugs. Left image: a single cell in untreated spheroids emanating from the original spheroid core. Right image: the elongated shape disappears after treatment with inhibitor and is replaced by a rounded phenotype. Fluorescent label: Alexa Fluor 488 phalloidin. Scale bar = 10μm. Colour bar: sample depth.

Figure 2. Representation of 2D and 3D output of the ImageJ plugin.

A. 2D analysis of individual slices. Left: original iSIM image. Right: graphical and text output from the plugin. White outline = identified object; blue circle = centre of mass of the outline; brown outline = sliding average of outline, estimated area of the cell body; yellow lines = radii of major protrusions from the centre of the estimated cell body. Scale bar = 5μm.

B. Projection of the Z-stack output from automated analysis of the entire Z-stack image of the cell in A. 3D image rotated for visualisation of the separate outlines per slice. Legend for output features as in A. Scale bar = 5μm.

Figure 3. Analysis of migratory U251 glioma cells.

A. A novel ImageJ plugin was used to identify major protrusions and filopodia in the cells. Asterisks (centre panel) indicate individual filopodia, Y-shaped structure highlights major protrusions. Major Protrusions: 3 Filopodia: 21. Scale bar = 10μm. B. Graphical representation of max projection 3D data generated from single cells, untreated versus treated, using iSIM and the ImageJ plugin. Fifty cells/condition were scored and the average is depicted in graphical format. Five biological replicates per condition were used with 10 technical replicates taken from each. Differences between control cells and treated cells were compared using a two-tailed *t*-test (Excel). Error bars were generated using standard error of the mean (SEM). Asterisks indicate statistical significance where **** = p≤0.0001.

Supplementary Figure 1. Parameters to be changed by the user in the graphical user interface (GUI) and resulting data generated by the plugin acting on an input image (top). The window length chosen by the user to define major protrusions ($Window_{major}$) and the sensitivity threshold value of *b*-ratio for detecting protrusions (dashed black line) are illustrated. Detection of protrusions by *b*-ratio (det) and localisation of them by maxima in *b*-product (max) are labelled in the graph. The plugin considers the outline as a closed polygonal line, and so the location of the third peak, i.e. the maximum in *b*-product between 'det 3' and 'det 1', appears before 'det 1' on the graph. E = eccentricity between perimeter and rounded perimeter, RP = rounded perimeter.

Supplementary Figure 2. A schematic diagram of the workflow for data analysis using the ImageJ plugin, 'Surface and DirectionDetector B' v1.0, available at https://github.com/rohwedderleeds/surfaceanalyser.

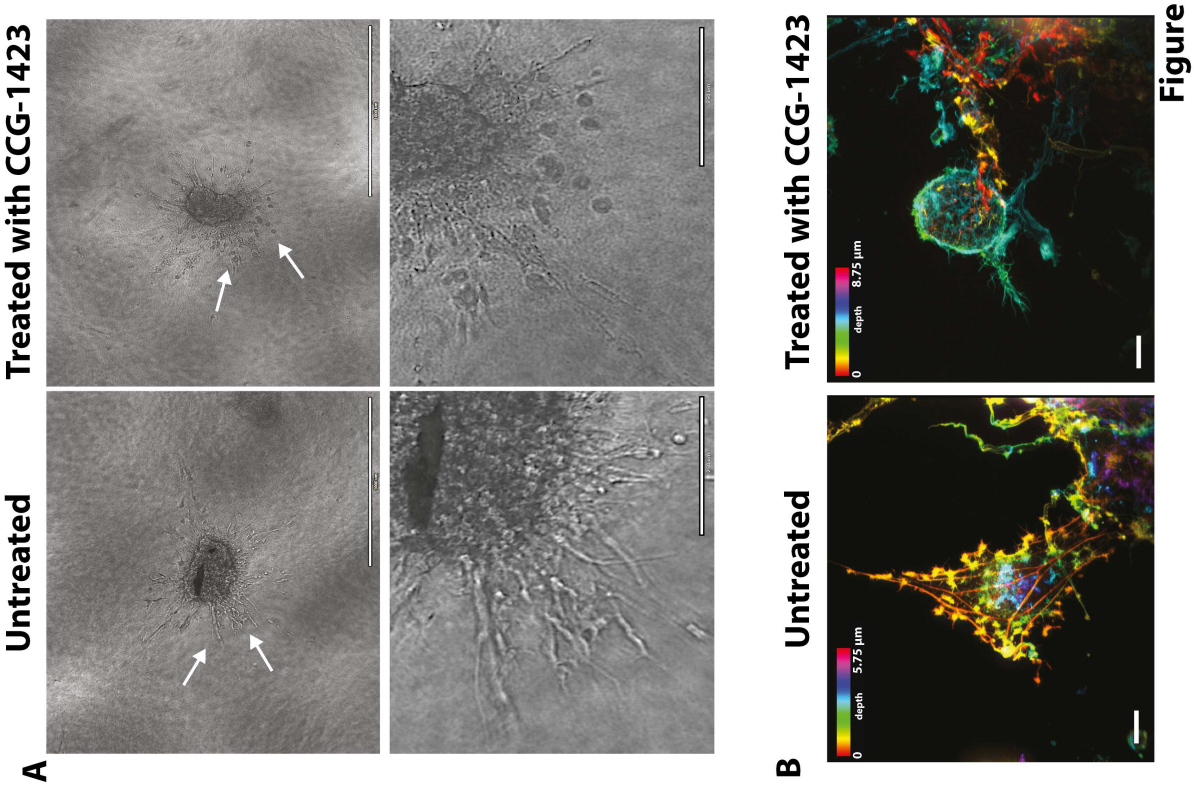
A
Untreated
Treated with CCG-1423
B
Untreated
Treated with CCG-1423
depth
0
5.75 µm
8.75 µm

Figure 1

A

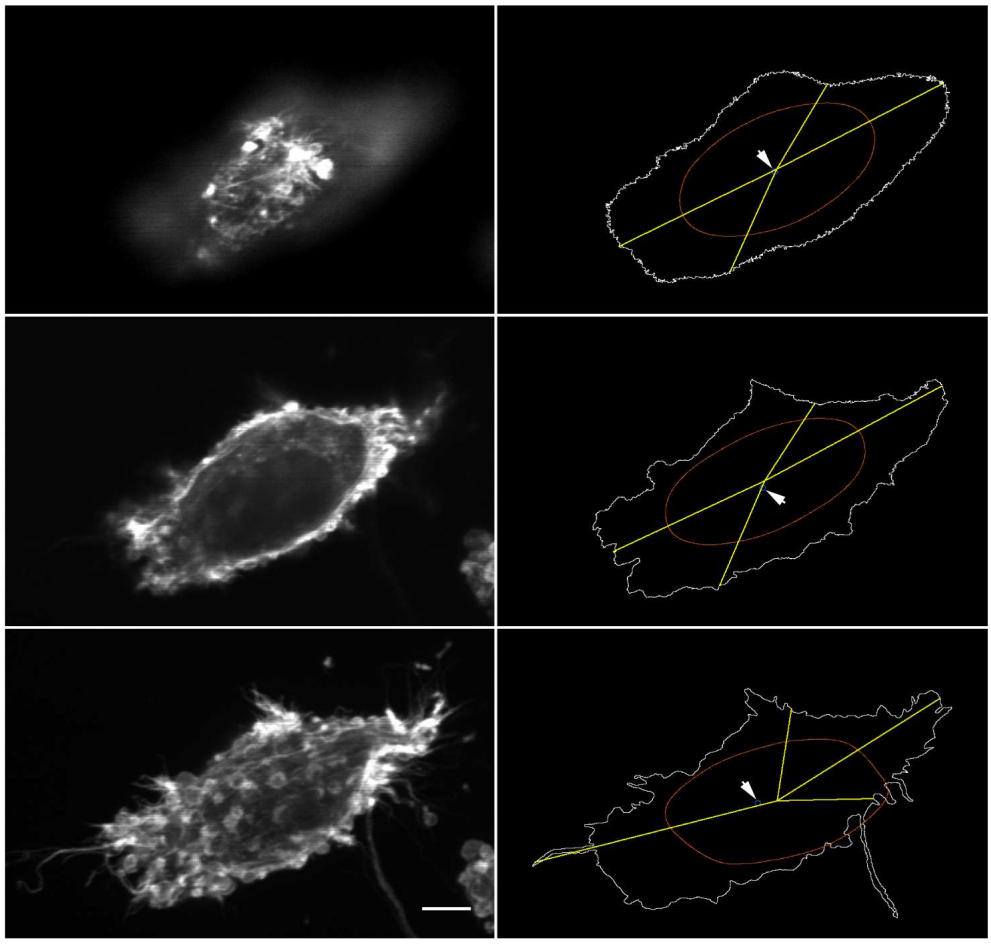
Image slice
Output
1.75 µm
4.25 µm
5.25 µm
Slice: 7
Eccentricity:
-0.22 µm horizontal
0.24 µm vertical
Major Protrusions: 4
Filopodia: 63
Slice: 17
Eccentricity:
-0.21 µm horizontal
0.68 µm vertical
Major Protrusions: 4
Filopodia: 52
Slice: 21
Eccentricity:
-2.01 µm horizontal
0.23 µm vertical
Major Protrusions: 4
Filopodia: 50

B

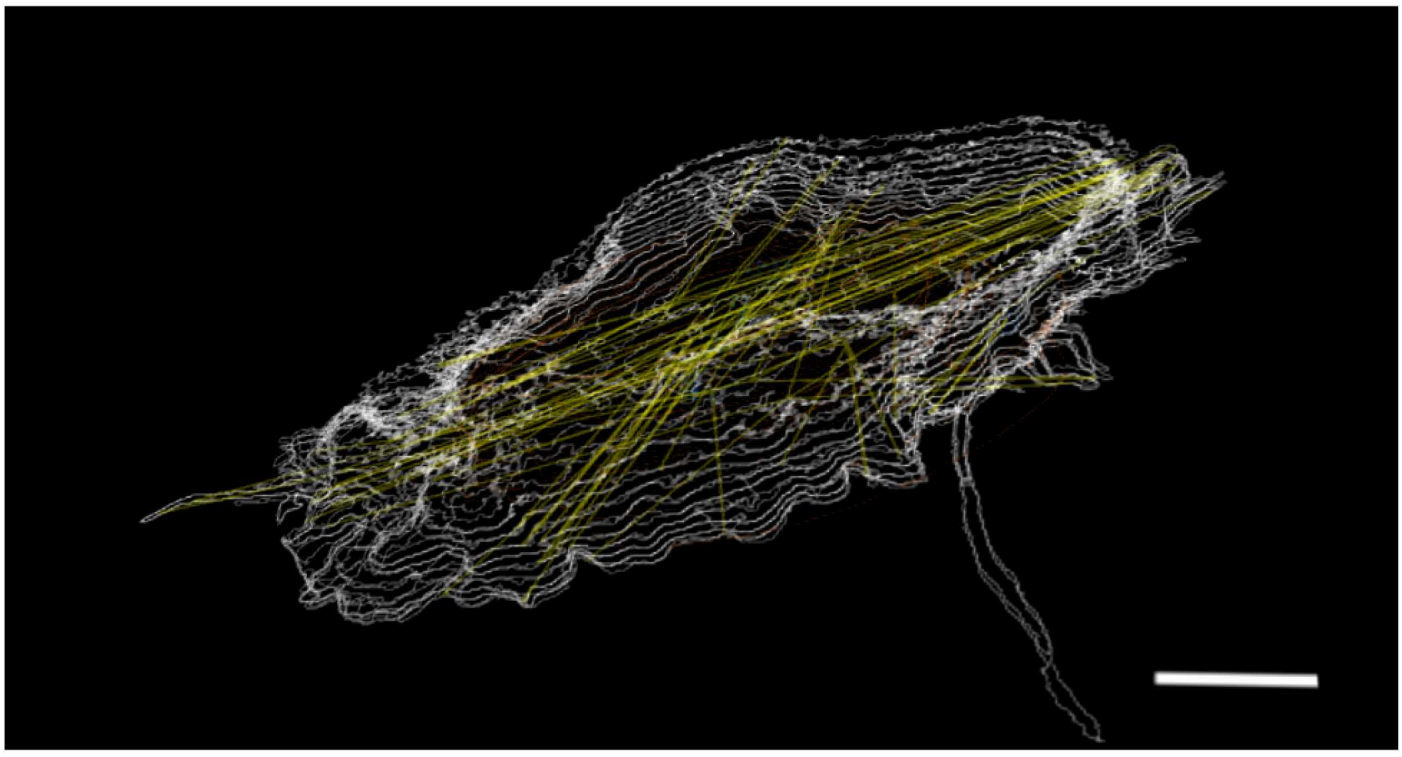
Projection of 3D output

Figure 2

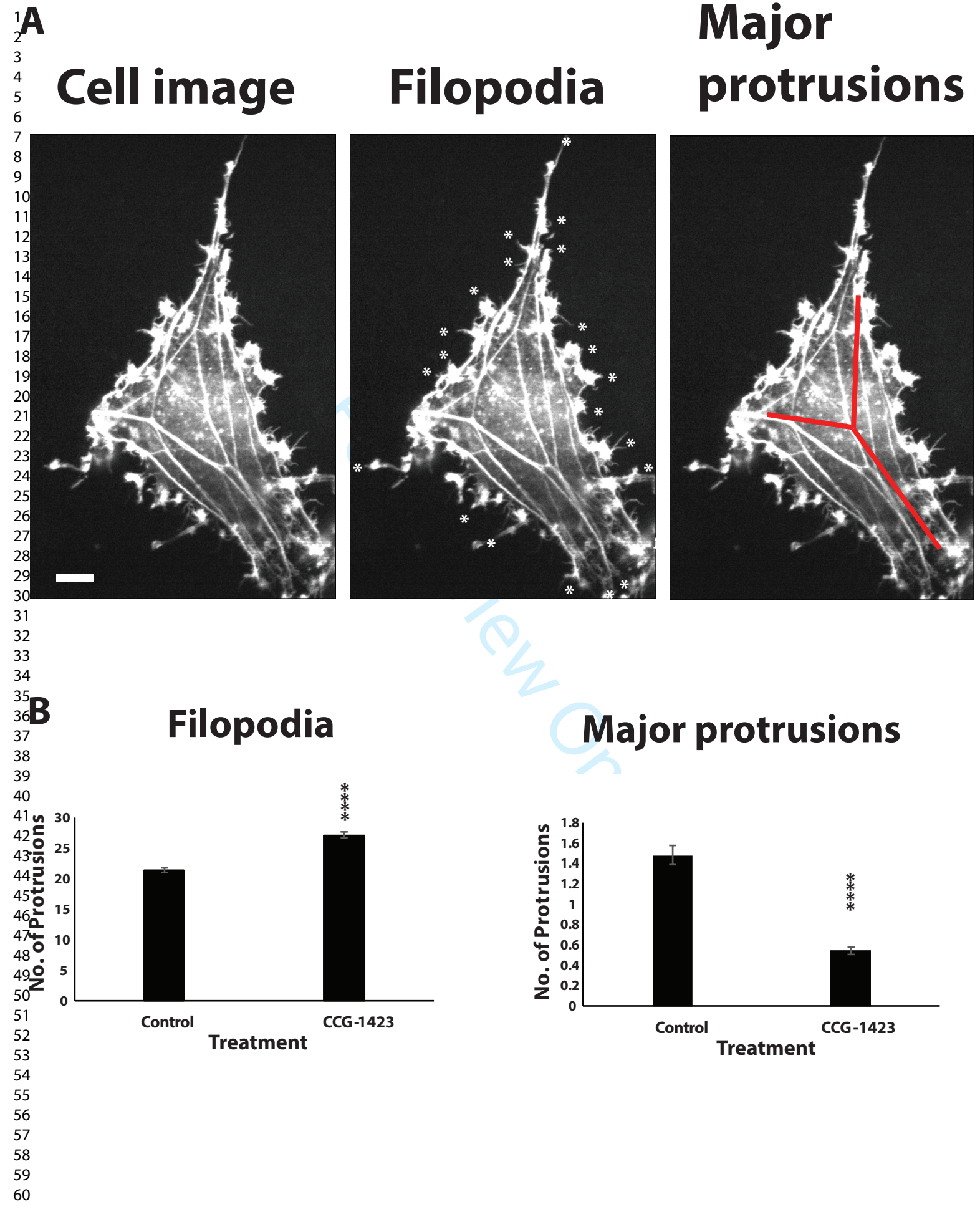
A
Cell image
Filopodia
Major protrusions
B
Filopodia
No. of Protrusions
30
25
20
15
10
5
0
****
Control
CCG-1423
Treatment
Major protrusions
No. of Protrusions
1.8
1.6
1.4
1.2
1
0.8
0.6
0.4
0.2
0
****
Control
CCG-1423
Treatment